



Sensitivity of a reinforced concrete protective gallery under a snow avalanche load

Dominique Daudon^{a,*}, Julien Baroth^a, Ying Ma^b, Pascal Perrotin^b, Michel Mommessin^b

^a UJF-Grenoble 1, CNRS UMR 5521, Grenoble INP, 3SR Lab, BP 53, 38041 Grenoble Cedex 9, France

^b LOCIE, UMR 5271, Université de Savoie, Polytech Annecy-Chambéry Campus Scientifique, Savoie Technolac, 73376 Le Bourget du Lac Cedex, France

ARTICLE INFO

Article history:

Received 5 July 2011

Received in revised form 21 September 2012

Accepted 24 September 2012

Available online 6 December 2012

Keywords:

Snow avalanche

Protection gallery

Finite element model

Probabilistic sensitivity study

Dynamic loading

ABSTRACT

This paper focuses on avalanche protection galleries. Horizontal and vertical structurally reinforced concrete elements are modelled herein using the finite element code (FE), under both static and dynamic avalanche loads. The variability of these loads is modelled using lognormal random variables, taking into account experimental data. A sensitivity stochastic FE analysis characterises the variability of the vulnerability indicators: maximum displacements or stresses in the concrete and reinforcement rods, showing that the variability of transient load components have a great impact on the variability of the indicators. These results confirm, contrary to current building codes, the need to take the dynamic behaviour of these galleries into account, in the design.

© 2012 Published by Elsevier Ltd.

1. Introduction

In the field of natural risk management, the vulnerability of protective engineering structures subjected to various phenomena, such as fire, flooding and earthquakes, may be defined to predict structural damage for a range of intensities found in the phenomenon considered. In the field of avalanche hazards, there are many technical solutions for protective measures, including civil engineering works: racks, nets, deviator dams or stop dams, etc. [1–3]. In particular, protective galleries are required to maintain road networks in any weather (avalanche protection and snow accumulation by wind). This paper focuses on the behaviour of snow galleries as presented in Fig. 1.

For many years, protective structures against avalanche flow have been designed using a static loading constant in space and time, based on the fluid mechanics equation of steady “shallow water” flow around an obstacle [4]. This static loading is considered by designers as equivalent to the avalanche load, but is based on an empirical approach with poor scientific basement.

The avalanche loads are a transient phenomenon but, in fact, this was not considered as for earthquake design loads in the Eurocode 8. However, as some structures were destroyed during the last decade in the Chamonix valley [6], large studies on the characterisation of the local stress and local velocity fields around the obstacle have been conducted, mostly in Europe. They evaluated

the transient impact effect, *i.e.* the dynamic loading encountered at the arrival of the flow against the structure, which could be more than ten times the static load calculated with a steady velocity [5–10,12]. Moreover, Thibert and Baroudi [13] confirmed recently that the maximum power of the avalanche is injected at the very beginning of the impact, when the head of the avalanche impacts the structure.

Whatever technical solution is selected, quantification of damage requires complex constitutive laws and models [14–16], in addition to knowledge of the potential real load. French and Swiss building codes are based on static design loads only, neglecting both the spatial and temporal variability of the snow impact loading and their effects [17–19]. The protective structure's natural period and the time to rise in load are about the same order, it is important to take into account dynamic effect of both load and structure. The analysis conducted on Taconnaz deviator “teeth” structures shows that the static loads taken into account for the design were not sufficiently relevant [6,18]. This event led to significant *in situ* research to improve the quantification of the forces impacted on structures. Experimental studies on reduced-scale structures located at Lautaret Pass (Cemagref's artificially triggered avalanche test site) were conducted to assess the temporal evolution of pressure and impact energy [20,5]. The impact of the currently defined design load was identified. Therefore, it seems crucial to take into account the dynamic and transient nature of the avalanche characteristics using the design features and if possible suitable numerical solutions [10,11,16–19].

With this aim in view, understanding the effect of the variability of uncertain input parameters on the mechanical response of

* Corresponding author. Tel.: +33 476 827 044; fax: +33 476 827 043.

E-mail addresses: Dominique.Daudon@ujf-grenoble.fr (D. Daudon), jbaroth@ujf-grenoble.fr (J. Baroth), ying.ma@hotmail.fr (Y. Ma), Pascal.Perrotin@univ-savoie.fr (P. Perrotin), Michel.Mommessin@univ-savoie.fr (M. Mommessin).



Fig. 1. Photo of the Montalever avalanche protective gallery.

the gallery is crucial. This requires classic studies to be completed using certain probabilistic approaches. Monte Carlo simulations are well-known, simple and robust methods [20], but despite their improvements (e.g. [21]), they are still time-consuming if the embedded deterministic model is complex. Therefore, alternative methods, called stochastic finite element methods (SFEM), have been proposed [22,23,28]. SFEMs are more relevant if the FE model analysed is mechanically nonlinear. In fact, when a linear mechanical model is used the variability of the output parameters is a linear function of the input one's giving less sense to the uncertainty characterisation of those models. In this paper, the SFEM selected is a collocation method [24] based on the quadrature method [25].

The first part of this paper presents the results of two experimental campaigns aiming to characterise the ratio between the tangential and the normal components of a flow load. The first was an in situ experiment of snow flows such as avalanches. The second one aims to quantify the variability of the ratio of the components of a dynamic bead flow load in a laboratory channel. These studies were part of the OPALÉ experimental project [40].

The second part focuses on finite element (FE) modelling of a typical recently built protective gallery, to quantify the dynamic effect, modelled in two different ways:

- the first used a research code, FEDEASLab [26], with a specific dynamical behaviour law for concrete; a simplified two-dimensional geometry was used (cf. Fig. 7);
- the second was based on a more realistic three-dimensional geometry but with an “industrial” code, ABAQUS [30], and constitutive behaviour law currently used for concrete structures [18].

The gallery structure was broken down into two sub-structures (the roof and the column): the roof was modelled as a simplified plate-beam and the column supporting the plate-beam roof as a three-dimensional solid supporting the dynamic load from the computation of the roof behaviour under the impact of a snow avalanche. The quantification of the mechanical vulnerability of the column finite element model is detailed. Its damage response consists of a number of vulnerability indicators, including maximum displacements or stresses in both the concrete and rods. The choice of these different types of indicators must reflect the complexity of the numerical model. The same indicators were chosen in [31] to study the vulnerability of structures taking into account the spatial variability of avalanche loading.

The third part aims at quantifying the sensitivity of the damage response of these structural elements to the variability of uncertain design parameters related to either the concrete or the actual avalanche load amplitude. These parameters could in fact differ slightly between the real structure and the results from the design step. In particular, the influence of the “ c ” parameter, which represents the ratio between the tangential avalanche loading to the normal loading is pointed out and is included in the design. As defined in the guidelines, this parameter was chosen between 0.3 and 0.4 (French and Swiss guidelines [4]) depending on the location of the slope change (cf. Fig. 2). Laboratory and in situ experi-

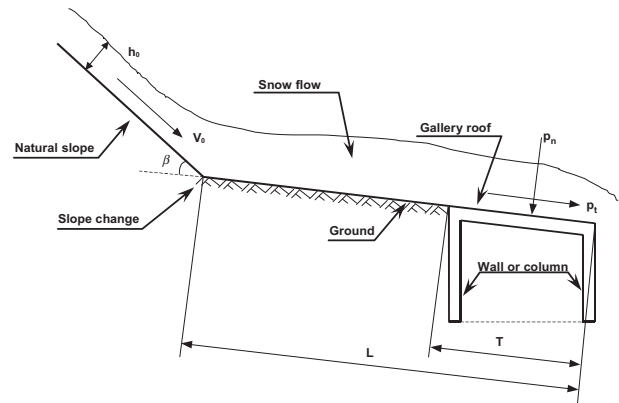


Fig. 2. Schema of the gallery parameters for the snow load calculation.

mental studies, [10] and [12], have shown that spatial and temporal variation of c and its effect on the damage of the structure is substantial: in fact, c could be considered a statistical distribution.

Sensitivity to numerical method parameters is also studied. Therefore, the influence of the number of points needed for the collocation method is analysed, and the type of the probability law of the input parameters is explored. Then a methodology is detailed in order to quantify the influence of the c coefficient.

This analysis shows that the variability of the horizontal dynamic load component and the ratio of the horizontal and vertical components have a great impact on the variability of the response indicators. These results confirm the necessity to take into account the dynamic behaviour of such galleries, contrary to current building references practices which take equivalent static loads.

2. Characterisation of the avalanche load

The loadings adopted here were contributed by the French OPALÉ research project. They come from experimental studies conducted over three winters on artificially triggered avalanches. The measurements were taken on a specially developed macro-sensor with the purpose of measuring avalanche loading in as similar a way as possible to the load exerted on a roof protection gallery. For further details see [10]. The roof of the gallery is subjected to a pressure load p_n and p_t , and the upper articulated column elements are submitted to point loads (vertical and horizontal) from the roof load transmission.

2.1. Static and dynamic snow avalanche loads

Two types of avalanche impact loads are applied, *i.e.*

- “Static peak” load is based on the peak pressure of the transient avalanche loading.
- “Transient dynamic” load: based on experimental measures taken at Lautaret Pass (winter 2007), this experimental record is used to analyse the transient effect on the behaviour of the modelled structure.

2.1.1. Static normative load design

The static normative load estimation is evaluated from the classic equation of steady dynamics of fluid pressure (ρV^2) considering the Voellmy formula [32] for the avalanche flow velocity (V) and density ρ .

The corresponding normal and tangential pressures loading the roof gallery, denoted p_n and p_t , are calculated by OFROU [4] as in Fig. 2.

Table 1

Normative pressure on the roof gallery and snow cover weight pressure, before and after avalanche flow. Two types of avalanche are considered: a current one (service pressure) and an exceptional one (exceptional pressure). The return period of the current avalanche is generally around 10–50 years, and less than the exceptional one (more than 100 years).

Type	Orientation	Service pressure (kPa)	Exceptional pressure (kPa)
Exceptional avalanche	Normal to the roof	6	14
	Tangential to the roof	2	5
Snow cover	Vertical	Initial 6, final 11	Initial 9, final 17

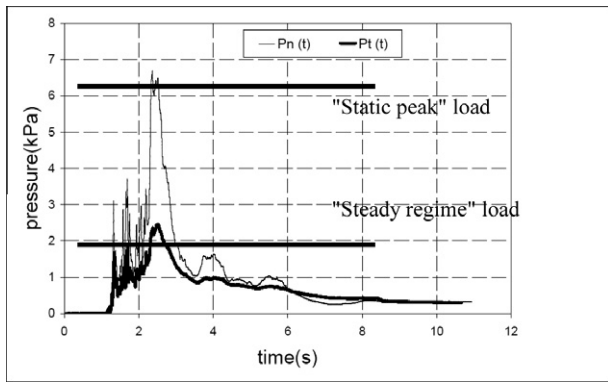


Fig. 3. Roof snow impact loading measured with a real avalanche and the associated static load pressures.

$$p_n = \frac{\rho V^2 h_0 \sin \beta}{L} \quad \text{and} \quad p_t = c \cdot p_n \quad (1)$$

where β is the deviation angle between the gallery and the ground slope (equal to 20°), h_0 an avalanche thickness before the break in slope (3 m), L the distance between the avalanche edge and the break in slope (around 20–25 m), and c a coefficient with a value between 0.3 and 0.4 depending on the snow type and geometrical situation. Far from the slope change, this coefficient is similar to a friction coefficient. In Switzerland it has recently been accepted that the range of the values of c could vary between 0.2 and 0.55 [12] from on-site and laboratory experiments, instead of regulatory values between 0.3 and 0.4 [4].

Using the following avalanche characteristics (avalanche velocity $V = 30$ m/s and snow density = 400 kg/m³), the normative pressure obtained for the Montalever gallery is given in Table 1 [33].

2.1.2. Transient avalanche load

As mentioned above, the dynamic loading comes from the Lautaret Pass experimental measurements of a “small” avalanche. Real measured pressures were magnified about 1.6 times before being applied to the roof gallery FE model. The roof loading can be seen in Fig. 3.

2.2. Variations of the c coefficient (ratio of p_t/p_n)

As seen above, a value for the c coefficient, the ratio of the tangential to the normal avalanche loading has to be selected for the design of the snow shed. Some studies in both the laboratory and in situ, on sand, beads or snow, have shown that the c coefficient varies with flow range temporal and spatial factors [10,12], velocity and snow liquid water content [38], giving values from 0.1 for dry snow to 0.7 for wet snow.

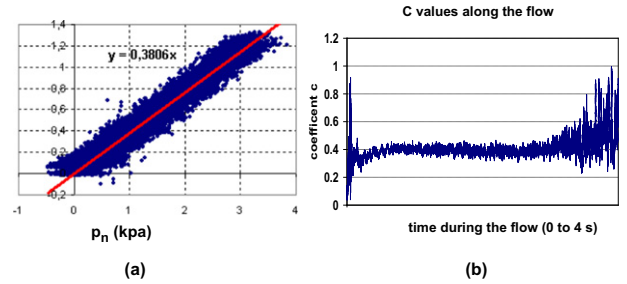


Fig. 4. Temporal evolution of p_t vs. p_n (a) and $c = p_t/p_n$ (0–4 s) in Ma Ying's laboratory experiments on a glass bead flow in a channel (b).

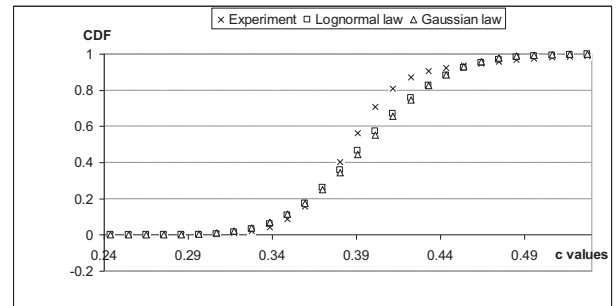


Fig. 5. Cumulative distribution function for c values with $x' = 1.67$.

However, c is also sensitive to the existence of a slope change in the flow pathway: as this change is near the gallery, an impact effect increases p_n and could change the c coefficient, as shown in Table 2 for the glass bead laboratory experiments [10]. The ratio is plotted by the p_n and p_t representations in Fig. 4(a) and the time history is presented in Fig. 4(b).

As the shed roof is far from the slope change, the c factor can be assumed to be a friction coefficient. This “far” condition is related to a distance L from the slope change more than five times the height of the flow, as stated in the snow shed guidelines [4]. Consequently, for the existing structures, it is important to lead on site maintenance to maintain fair topography: in effect, snow and debris upstream of the gallery can modify the topography and create a potential danger; this change has been quantified with laboratory studies using well-controlled parameters. Granular flows of glass beads have been generated in an instrumented channel, measuring p_n and p_t with time and position [11].

Stakeholders need to know how to optimise the design of the structures that may undergo variability of this coefficient c . Consequently, it is relevant to study the sensitivity of the structure's behaviour with c variability, even if the sources of variability are numerous and cannot be completely characterised.

2.3. Statistical approach of the experimental values of c

As seen in Fig. 4(b), the set of 22,000 experimental values of p_n and p_t measured near the slope change ($x' = 1.67$) is relatively homogeneous, giving a mean value of 0.38, but it seems relevant to remove negative values of c (due to the impact effect near the slope change) and the extreme values of the set (see large perturbations at the end of the history, Fig. 4(b)). Considering the restriction of the statistical set to the more pertinent values, mean values, standard deviation and density of probabilities were evaluated. A population of 18,000 positive values of c was used, with a mean equal to 0.41. The standard deviation was 0.07 (17%). The density

Table 2
Experimental values of c from Ma Ying's laboratory experiments on bead flow in a 4-m-long channel [10].

Position of the sensor with respect to the slope change	Close		Far
Dimensionless position x' of the slope change	1.67	3.33	5
Mean $p_t/p_n = c$ ratio for entire flow duration (0 – 4 s)	0.38	0.72	0.58
Mean of c for values restricted to steady flow duration (0.5 – 3 s)	0.41	0.61	0.65
Standard deviation (coefficients of variation) of c for values restricted to steady flow duration (0.5 – 3 s)	0.07 (17%)	0.14 (23%)	0.13 (20%)

Notes: x' is a dimensionless number equal to x/h_0 , x is the position of the sensor centre with respect to the slope change, h_0 is the height of the flow before the slope change.

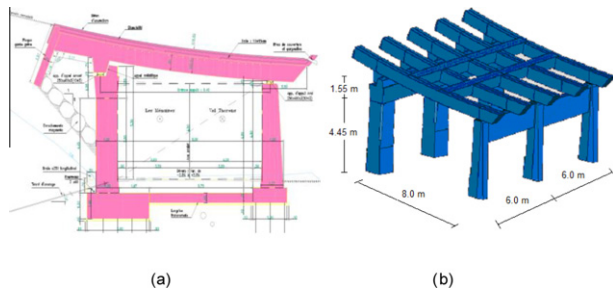


Fig. 6. Schematic view of the gallery section (a) and characteristic sequence of the tunnel and components (b).

of probabilities was computed considering a distribution of values covering a range of 4 standard deviations around the mean value. This range was divided by 40 intervals to plot the distribution.

Fig. 5 shows the changes in cumulative distribution functions with $x' = 1.67$, for experimental values and for normal and lognormal laws, with the same mean, 0.41, and standard deviation, 0.07 obtained by the calculus.

The normal and lognormal changes were close, but the match between experimental and theoretical changes is obviously not very good. Nevertheless, it seems valuable to consider more particularly the lognormal distribution of the ratio $c = p_t/p_n$. Indeed, the last section shows that giving a precise characterisation of the distribution of c is not realistic, given the numerous sources of uncertainty. Moreover, if distributions of p_t , p_n are considered log normally distributed, then the ratio $c = p_t/p_n$ is log normally distributed. It is why first the influence of p_t and p_n will be studied before studying the influence of c on the mechanical behaviour of the protection gallery, which is described in the following section.

3. The Montalever avalanche protection gallery: dynamic behaviour and vulnerability indicators

The aim of this part of the modelling process is to confirm the existence of a dynamic effect due to the snow avalanche loading on the structure. The structure is presented and we then focus on the material models and geometries, before comparing the results between the different loading cases (normative, static, dynamic). Two cases are modelled: simplified dynamic modelling of the roof in order to examine the damage in this part of the structure and to repair the columns [34,35,37]. The columns are then modelled using a more sophisticated model.

3.1. Presentation of the structure

The present study is based on a typical avalanche protection gallery. The model was inspired by the Montalever tunnel, which is one of the largest structures constructed in France over the past few years. It was designed to protect roadways in the French Alps (departmental road no. 117, near Saint Martin de Belleville). Snow avalanches are likely to occur there. The 490-m-long gallery is lo-

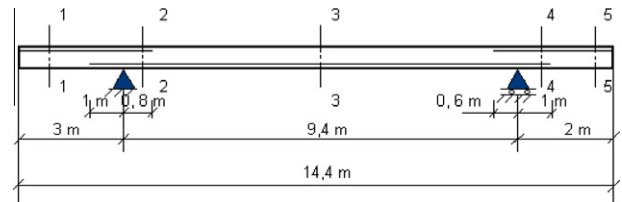


Fig. 7. Simplified schematic model for the computation (no transverse rods).

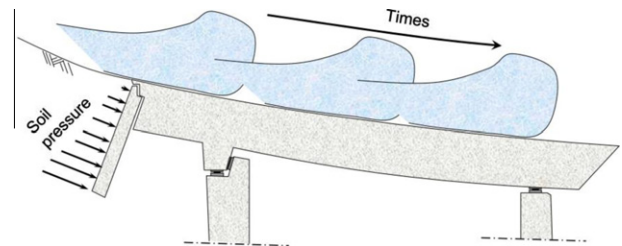


Fig. 8. Simplified model of the roof interaction with the column on the left and simple connection on the right showing avalanche loads at various points in time.

cated at the average altitude of 2100 m and is composed of reinforced concrete sub-structural elements (beams, columns, foundations) and a roof slab. The avalanche load comes from the upper slopes and will impact the roof structure with a normal and tangential load. The model of the structure is simplified, and neither the curvature of the roof nor its slope is considered. As it is a long structure, only a typical slice between two expansion joints is studied in order to compute the loading and the behaviour (Fig. 6).

3.2. Dynamic modelling of the roof

3.2.1. Geometry, boundary conditions

To be able to apply complex avalanche loading (varying in time and space), a simplified 2D model based on a Timoshenko multi-fibre beam was used [29]. The simplified 2D model is a homogenised beam equivalent to the slab and the longitudinal beams. The transversal rigidity is not taking into account because no variation of transversal load is considered. The beam was 14.4 m long, 0.35 m thick and 1 m wide (Fig. 7). Different distributions of longitudinal ribbed bars divided the structure into five different sections (Fig. 7 and Table 3). Plane strain deformation was assumed in accordance with the same width as the real structure. The connection with the upper stream pole was simplified to a ball joint and the connection with the downstream pole was a simple support (Fig. 8).

3.2.2. Loads applied to the structure

Given the natural period of the structure (0.2 s) and the duration of the load peak (approximately 0.1–1 s depending of the peak as to be seen in Fig. 3), the dynamic effect could influence the

Table 3
Ribbed bars in each section (HAxx: ribbed bars of xx mm of diameter).

	Section 1	Section 2	Section 3	Section 4	Section 5
Upper	4HA16 + 4HA20	4HA16 + 4HA20	–	8HA12	8HA12
Lower	–	8HA25	8HA25	8HA25	–

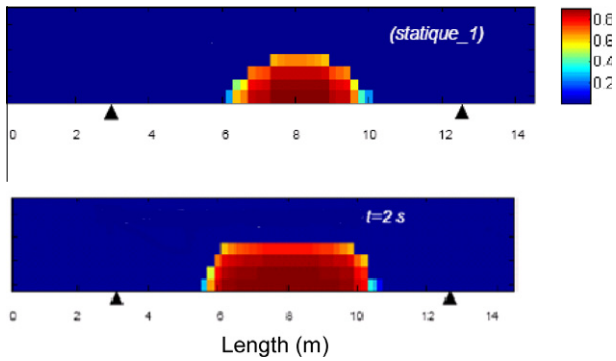


Fig. 9. Comparison of the damage zone of the beam (D_1 value) under static loading (above) and the transient dynamic loading (below), showing the superiority of dynamic loading in damage quantification.

behaviour of the protective structure. So it seems necessary to verify this influence and to examine and compare two loading cases:

- (1) “Static peak” load define before (Section 2.1): it is fixed at the maximum value of the transient load. This static load is constant across the width (dimension T of Fig. 2) of the protective structure.
- (2) The avalanche loading varied in time and space as it flows along the roof.

The applied roof pressure was one of the pressures measured at the Lautaret Pass [10]. It is magnified in order to obtain plasticity within the horizontal structural concrete components and to study the influence of the dynamic aspect on the roof.

3.2.3. Material models

The multi-fibre beam component is an FE based on the theory of beams in which each section is divided into fibres. In each fibre, a local constraint deformation constitutive law can be associated (see [10] for a more detailed explanation). It is therefore possible to model several different materials and the element section may be heterogeneous and non-symmetrical. In the present study, each fibre is either a constitutive law of concrete or steel is applied, so that a reinforced concrete material is simulated. The La Borderie damage law [35] is used for the concrete and the Menegotto Pinto model [36] is applied for the steel. A detailed description of the material model parameters is given in [10].

3.2.4. Results

Fig. 9 shows the damage variables of the concrete D_1 value on the beam under static and dynamic loadings (D_1 : tensile damage factor of Laborderie Law for the concrete [35]). It illustrates the greater damaged area of the “beam shell” computed for the real dynamic load obtained after the peak (at a time equal to 2 s) in comparison to the damaged area obtained for the static loading.

From the comparison between stresses and the displacement effect in the two load examples, it could be proposed that the effect of the transient load is equivalent to a static load value equal to the transient peak load magnified 1.6–1.8 times. In other words, a security coefficient of 1.6–1.8 should be applied to the maximum

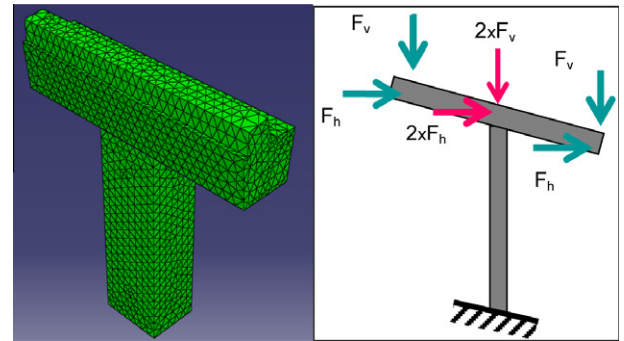


Fig. 10. 3D FE model of a column (left), boundary conditions and loads (right): $2 \times F$ load applied to the column and F applied between two columns. For each force, vertical and horizontal components (F_v and F_h , respectively) are depicted. We suppose a non affected transmission from the upper beam support to the column due to dynamic effects.

temporal value if used as a static value loading for the gallery design.

3.3. Dynamic modelling of a column

Here we focus on modelling a component of the structure: an upstream column of the snow shed. This column is loaded by the avalanche flow by expecting an articulated load transmission from the roof: horizontal and vertical loadings.

3.3.1. Geometry and boundary conditions

The geometry of the structure is depicted in Fig. 10. The model features two main components: the 4.45-m column height with a cross-section equal to 1.8 m^2 , and the 6.0-m-long transverse beam (cross-section, 1.1 m^2). The boundary conditions applied to this model correspond to the column’s position within the real structure. The bottom of the column is assumed to be embedded. The transverse beam part was only fixed in the horizontal direction in order to represent symmetry/continuity conditions. The numerical model consists of four-node tetrahedral elements for the concrete column and linear elements for the steel rebar reinforcement. The approximate overall size of the components was 0.2 m. The reinforcement is defined as wire elements bonded to the existing concrete. Only the primary reinforcement component was represented.

3.3.2. Applied load

We take into account the dead weight W of the structure, the earth pressure E generated from the soil located behind the snow shed, and the avalanche impact $y(t)$, in considering the dynamic feature of this load.

The dead weight $W = 237.5 \text{ kN}$ (roof, main beams and cross-beams) is applied to the column as a vertical reaction. The earth’s pressure introduced stems from indirect loads acting on the column, such as vertical and horizontal reactions. These reactions equal $E_v = 62.3 \text{ kN}$ and $E_h = 57.3 \text{ kN}$.

From the FE calculation of the roof, a load on the column component was calculated. This transient profile, shown in Fig. 11, de-

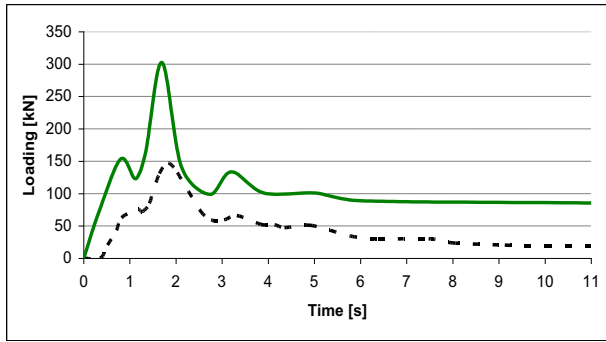


Fig. 11. Profiles for dynamic reaction forces loading from a calculation featuring the Lautaret Pass avalanche pressure: vertical (continuous line) and horizontal (dashed line) components.

Table 4

Characteristics of concrete parameters chosen for modelling [15]. Maximal tensile stress is 2.84 MPa and maximal compressive stress is 50 MPa (see abaqus manual for more information).

Young modulus	$E = 30$ GPa	$\sigma_{bo}/\sigma_c = f$	$f = 1.12$
Poisson coefficient	$\nu = 0.19$	Angle of dilatation	$\beta = 38^\circ$
σ_{bo}, σ_c : compressive stresses (plastic maximal and initial elastic)			
Compression		Tension	
Stress [MPa]	Plastic strain [10^{-3}]	Stress [MPa]	Plastic strain [10^{-3}]
15.0	0.0	1.999	0.0
20.20	0.0747	2.842	0.0333
30.0	0.0988	1.87	0.160
40.30	0.154	0.871	0.280
50.01	0.762	0.226	0.685
40.24	2.56	0.0566	1.08
20.24	5.68		
5.258	11.7		

Table 5

Parameters of the steel plasticity model.

Young modulus E [GPa]	210
Poisson ratio ν [–]	0.19
Yield stress [MPa]	500

scribes both the normal and tangential loads finally applied to the up slope gallery column. The resultant vertical loads of $2 \times F_v = 432$ kN and $F_v = 237.5$ kN, respectively, are then applied to each column and the extremities of the transversal beam between to columns.

A static comparison is also made in the following section by considering both a static load equal to the peak value of the impulse load, and a steady regime value from the estimation of the steady state load after a time equal to 4 s.

3.3.3. Material models

We consider a nonlinear constitutive law for both concrete and ribbed bars in order to describe the structural behaviour in the ultimate state. The constitutive parameters correspond to the C50 concrete class (i.e. 50 MPa 28 days compression load strength) and are listed in Table 4 and implemented in Abaqus's Concrete Damage Plasticity (CDP) constitutive model [15] chosen for this purpose. Both compression hardening and tension stiffening of the concrete are taken into account.

The classic Mises elastoplasticity model used in steel construction is applied here for the reinforcement rods (Table 5).

3.3.4. Results

Table 6 compares the values of vulnerability indicators for an actual transient load and a static load equal to the transient load peak and a static normative design load (see Section 2.1). The vulnerability indicators are: the maximum Von Mises stress in steel rod, maximum concrete stresses (both compressive and tensile), maximum displacement (column head), and plastic strain (in the concrete column bottom). This table presents indicators that are greater for a dynamic load than a reference steady regime static load, but only the plastic strain indicator is greater under the transient loading than under the static load impulse peak value, demonstrating the larger damage of dynamic loading vs. static ones. These results are part of a more comprehensive study [18] that demonstrated that a static analysis should be complemented by a dynamic analysis, as a result not only of these greater values, especially considering the plastic strain in the concrete column (Table 6), but also because of the need to adapt reinforcement rod geometry to dynamic action. The concrete can also be damaged before reaching the static reference load. Moreover, it seems worthwhile to study the sensitivity of such a dynamic load to the variability in material parameters.

4. Probabilistic approach of the dynamic real snow avalanche

4.1. Position of the problem

The uncertain input parameters are the dynamic loads, modelled by random processes, depending on random variables Y_1 and Y_2 . These input random variables are gathered in the vector $\mathbf{Y} = \{Y_1, Y_2\}$ with a known probability law. The vulnerability indicators of the column consist of the Von Mises stress in ribbed bars, stresses in concrete, maximum column head displacement and maximum plastic strain in concrete. These uncertain output parameters are modelled by the random vector $\mathbf{Z} = \{Z_1, \dots, Z_S\}$ to be characterised.

The FE model is represented as a function f , such that $\mathbf{Z} = f(\mathbf{Y})$. Let g be the composite function ($f \circ T$) of the mechanical response function f , linking \mathbf{Z} and \mathbf{Y} , and the function T linking \mathbf{Y} with a standard random variable \mathbf{X} (Gaussian), such as $\mathbf{Z} = g(\mathbf{X})$ [24].

4.2. Probabilistic method

For the sake of simplicity, let us consider only the scalar output $Z = Z_1 = Z$. The mean μ_Z and standard deviation σ_Z of Z are approximated such that:

$$\tilde{\mu}_Z = \sum_{i=1}^N \omega_i \cdot g(x_i); \quad \tilde{\sigma}_Z^2 = \sum_{i=1}^N (g(x_i))^2 \cdot \omega_i - (\tilde{\mu}_Z)^2 \quad (3)$$

with N points and weights $(x_i, \omega_i)_{1 \leq i \leq N}$ that can be found in [27]. The coefficient of variation of Z , denoted $Cv(Z) = \sigma_Z/\mu_Z$, can therefore also be approximated.

In addition, the mechanical response Z may be approximated using these points and weights, in writing the approximation \tilde{Z} of Z as a development of Lagrange polynomials [24], denoted L_i where for this study i varies from 1 to N :

$$\tilde{Z}(x) = \sum_{i=1}^N g(x_i) \prod_{\substack{k=1 \\ k \neq i}}^N \frac{x - x_k}{x_i - x_k} = \sum_{i=1}^N g(x_i) \cdot L_i(x)$$

Monte Carlo simulations might eventually be applied to this response surface in order to obtain an approximation p_Z of the probability density function (PDF) p_Z . From this PDF, the probability $P(z < z^*)$ of remaining below the limit value z^* can be evaluated, this probability being not less than a few percent [39].

Table 6
Comparison of vulnerability indicators from static and dynamic analyses.

	Static load [ref. avalanche i.e. equivalent steady regime] (real avalanche peak)	Transient load (from Fig. 11), magnified as explained Section 2.1.2
Steel max. Von Mises stress [MPa]	[18.2] (55.9)	40.7
Max. concrete compressive stress at the foot of the column [MPa]	[6.9] (10.6)	9.8
Column head max. displacement [mm]	[1.3] (5.3)	3.6
Concrete max. tensile plastic strain [10^{-5}]	[57.6]	194

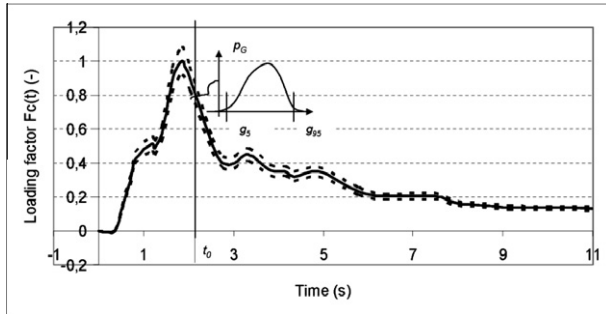


Fig. 12. Example of the 90% confidence interval around the average loading factor $F_c(t)$ deduced from the approximated avalanche load [10]. The probability density function p_G of $G \times F_c(t_0)$. If $t_0 = 7.5$ s, whereas $F_c(t_0) = 0.2$, the random variable $G \times F_c(t_0)$ is characterised by the mean 0.2 and standard deviation $0.2 C_v(G)$.

4.3. Modelling the variability of the components of the snow avalanche

In this section, the variability of the components of the snow avalanche presented in Section 2 is modelled. The uncertain parameters considered are vertical and horizontal components $y_v(t)$ and $y_h(t)$ of intensity $y(t)$ of the dynamic real snow avalanche, such that:

$$y(t) = \sqrt{y_v^2(t) + y_h^2(t)} \tag{5}$$

Let $Y_v(t)$, $Y_h(t)$, be the random processes modelling the vertical and horizontal components, respectively. If $Y_v(t)$ and $Y_h(t)$, modelling $y_v(t)$ and $y_h(t)$, are lognormal random processes, then the $C(t) = Y_h(t)/Y_v(t)$ ratio is also a lognormal random process. The effect the variability of the c ratio can therefore be studied as well. To approximate $Y_v(t)$, $Y_h(t)$ with lognormal processes, let G be a lognormal random variable of mean 1 and standard deviation σ_G , such that each process $Y_i(t)$, ($i = h, v$) can be arbitrarily approximated by the product $G \times y_i(t)$.

Fig. 12 describes the temporal evolution of the load factor $F_c(t) = y_i(t)/\text{Max}[y_i(t)]$, $t \in [0, 11]$ s]. At a given time t_0 , the PDF of the random variable $G \times F_c(t_0)$ can be defined. The graph of this function PDF ($G \times F_c(t_0)$) is plotted against $g \times F_c(t_0)$ realisations. In particular, g_5 and g_{95} represent the 5% and 95% fractiles of the random variable G , respectively. Thus, g_5 (resp. g_{95}) is the value of $G \times F_c(t_0)$ greater than 5% of the realisations of $G \times F_c(t_0)$ (resp. 95% of the realisations).

4.4. Sensitivity analysis of the FE model

This section presents the effects of horizontal and vertical components of the avalanche load on the vulnerability indicators of the FE model of the gallery column. The influence of the distribution type (normal or lognormal) and the influence of the number of collocation points are also studied.

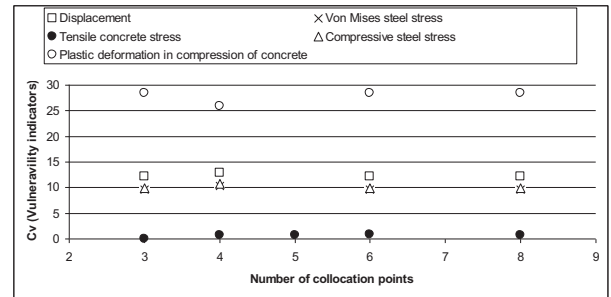


Fig. 13. The C_v of vulnerability indicators vs. the number of collocation points (Cv horizontal dynamic load: 10%).

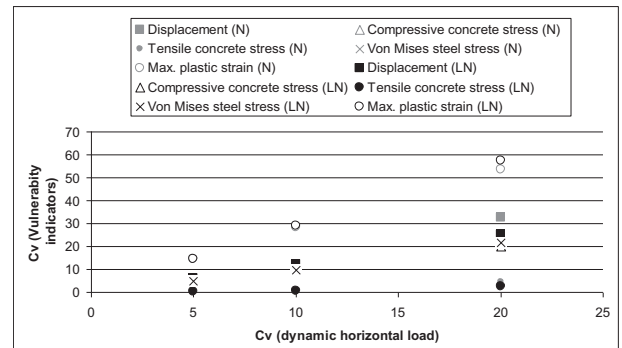


Fig. 14. The C_v (coefficient of variation) of vulnerability indicators for different C_v of the dynamic horizontal load, for normal and lognormal distributions.

4.4.1. Effect of horizontal load variability

The horizontal component of the load is denoted avalanche $y_h(t)$. Its maximum is defined by the product of the peak of the force applied to the column horizontally (225 kN; see Fig. 11), and a safety factor of 1.5. The function $y_h(t)$ is modelled by a random process $G \times y_h(t)$, where $G \sim LN(1, \sigma_G^2)$. The average mechanical responses are more consistent in the coefficients of variation.

Fig. 13 presents the evolution in the coefficient of variation (C_v) of vulnerability indicators, for different numbers of collocation points.

We first consider arbitrarily that the horizontal load is modelled by a normal distribution and that its coefficient of variation is equal to 10%. We note that all coefficients of variation (C_v) of the vulnerability indicators are nearly the same, whatever N is between 4 and 8. $N = 4$ or $N = 6$ seem to be enough to proceed.

Fig. 14 presents the coefficient of variation (C_v) of vulnerability indicators for different coefficients of variation (C_v) of the dynamic horizontal load, for normal and lognormal distributions, for $N = 6$ collocation points. Even if the coefficient of variation of the dynamic horizontal load is equal to 20%, there is not a significant effect of the distribution type.

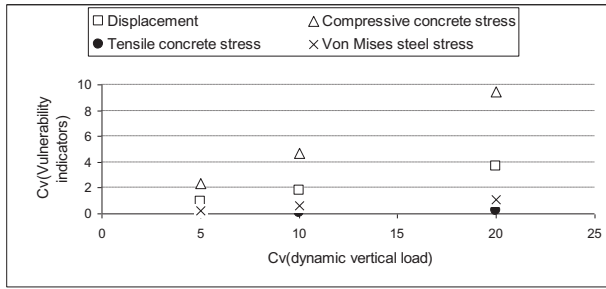


Fig. 15. Coefficients of variation of vulnerability indicators vs. coefficients of variation for the vertical dynamic load.

Fig. 14 shows that displacement and maximum plastic strain in concrete are particularly sensitive to variations in the horizontal avalanche component. The coefficients of variation for these parameters are thus more than 50% and 20%, respectively, for a 20% variation in horizontal load.

Horizontal load variations, however, do not appear to significantly influence the variability in concrete tensile stress f_t . For example, probabilities can be quantified in order to observe a tensile stress of up to 3 MPa, as denoted $\Pr(f_t > 3 \text{ MPa})$; these values equal 0.58% and 3% for horizontal load variations of 10% and 20%, respectively.

4.4.2. Effect of vertical load variability

Let us consider the effect of vertical avalanche load component $y_v(t)$. The function $y_v(t)$ is modelled by a random process $G \times y_v(t)$. The vulnerability indicator means are nearly constant, even though the coefficients of variation increase from 5% to 20%. The mean Von Mises stress in ribbed bars equals 40.7 MPa, while the mean maximum tensile stress in concrete is 2.93 MPa and the mean maximum compressive stress in concrete is 9.8 MPa. The mean of the maximum column head displacements is equal to 3.66 mm. Fig. 15 depicts the changes in the coefficients of variation for displacement, Von Mises stress and concrete compressive stress for different coefficients of variation specific to load intensity. The linear relations and the strong dependence of compressive stress can be noted, along with a non-significant dependence of displacement and Von Mises stress.

4.4.3. Modelling the variability of the ratio of the snow avalanche components

This section presents strategies to represent the variability of the ratio $c(t) = y_h(t)/y_v(t)$, where $y_v(t)$ and $y_h(t)$ are vertical and horizontal components, respectively, of the intensity $y(t)$ of the dynamic real snow avalanche, with $t \in [0, 12 \text{ s}]$. The condition (1) is then written such that:

$$y_h(t) = \frac{c(t)y(t)}{\sqrt{1+c^2(t)}} \quad (6)$$

where $c(t)$ is included in the interval $I = [0, 2; 0, 8]$, from experimental data (Fig. 4). If $Y_v(t)$ and $Y_h(t)$, modelling $y_v(t)$ and $y_h(t)$, are log-normal random processes, then the $C(t) = Y_h(t)/Y_v(t)$ ratio is also a lognormal random process. Let each process $Y_i(t)$ be arbitrarily approximated by the product $Y_i \times y_i(t)$, where $Y_i \sim LN(1, \sigma_{i2})$, the $C(t)$ ratio can be written $c(t) \times Y_h/Y_v$, where $Y_h/Y_v = L \sim LN(\mu_L, \sigma_L^2)$, such that:

$$\mu_L = (1 + \sigma_v^2)(1 + \sigma_h^2) \quad (7)$$

$$\sigma_L^2 = \mu_L^2 [(1 + \sigma_v^2)(1 + \sigma_h^2) - 1] \quad (8)$$

First strategy. From these last sections, it seems that the effect of the horizontal load is greater than the vertical load. Moreover, if σ_v is considered insignificant compared to σ_h from Eq. (8), we can deduce that the variability of the horizontal load gives a good idea of the variability of the ratio $c(t)$. Vulnerability indicators (as maximum displacement or plastic strain in concrete) are also highly sensitive to the $c(t)$ ratio.

Second strategy. Let us consider that the original resultant loading value should be respected in terms of direction and resultant load. The four collocation point loading approximations should be computed at each time step of the loading. This strategy introduces uncertainty at each time step respecting the same mean direction given by the c instant value and the mean instantaneous resultant values of the avalanche loading.

At time step t_i , the y_{vi} and y_{hi} loading values give a c_i factor and resultant

$$R_i = \sqrt{y_{vi}^2 + y_{hi}^2} \quad (9)$$

The Gauss points j approximation of the loading at time i is calculated using a given covariance on c_{ij} and calculating the y_{1ij} and y_{2ij} loading by resolving the two following equations:

$$y_{hij}/y_{vij} = c_{ij} \quad \text{and} \quad \sqrt{y_{vij}^2 + y_{hij}^2} = \sqrt{y_{vi}^2 + y_{hi}^2} = R_i \quad (10)$$

This strategy implies that the uncertainty on c will lead to an uncertainty restricted to the direction of the resultant snow loading without changing the resultant loading. Whereas the first strategy could imply an uncertainty of c due to a variation in the component of the loading, this last strategy simultaneously leads to a variation in the resultant of the snow loading and to the variation of c .

A comparison of the two strategies is given in Table 7. One can note that the first strategy (horizontal loading only) gives quite great values of the vulnerability indicators especially for the concrete ones (max. displacement, max. compressive stress, max. tensile plastic strain). The second strategy minimises those precedent indicators but emphasises the steels rod ones. As the first strategy corresponds to a “ c ” value equal to 1 and the second strategy is a c regulatory chosen value one could suggest to do calculus for both c values, and to have an expert analysis of the two results, depending on what is pertinent for the structure.

In fact, as this study is done for structures elements perpendicular (vertical) to the avalanche flow the expert analyses of results may be done for a $c = 0$ (vertical loads i.e. flexion loads only) and the same c reglementary chosen values as formerly proposed. However, compute the structures elements first with their most damaging load, i.e. $c = 0$ or $c = 1$ depending on the structure element characteristics by the flow direction could be a first way of a preliminary design.

5. Conclusions

In this study, several FE calculations were carried out under dynamic loads of real avalanches and under static loading. The objective was to focus on the vulnerability of mechanical structures such as avalanche-type galleries. This vulnerability was mechanically characterised using several indicators: the maximum stresses and displacements in concrete, the size of the damaged zone, and plastic deformation in the compression of concrete. Several static and dynamic loads were compared in terms of real vulnerability. These models, even simplified, helped to highlight the substantial influence of the dynamic nature of the load on the behaviour of avalanche structures. The dynamic effect then has to be considered in the design at four levels:

Table 7Comparison of vulnerability indicators for a 10% covariance for c at each loading time for both strategies and both normal and lognormal laws.

	Max. displacement [mm]	Max. concrete compressive stress [MPa]	Max. concrete tensile stress [MPa]	Max. Von Mises stress [MPa]	Max. tensile plastic strain (concrete) [10^{-5}]
First strategy lognormal Law	12.21	9.92	0.77	4.77	28.5
Second strategy lognormal Law	5.59	2.24	0	7	7.45
Second strategy normal law	6.65	2.80	1.26	9	9.78

- It acts specifically on the extent of the damaged area and its moment of occurrence.
- It operates on the maximum displacements and maximum stresses of the structure under a static load corresponding to a steady state. This static load, assuming the definition of reference load, is insufficient in amplitude to obtain the maximum values for an actual avalanche.
- The ratio between the normal and horizontal component of stress influences the maximum values of the indicators of vulnerability, this ratio changes during the avalanche (high during the initial shock) and possibly during the life of the structure. The study of the sensitivity of the FE model highlights a predominant sensitivity of maximum displacement and plastic deformation in the compression of concrete, particularly in the horizontal load and the c ratio.
- The structure can be loaded in an oscillatory manner, which means taking the corresponding constructive features into account (possible fatigue behaviour over the life of the structure, lifting components, geographic distribution of suitable reinforcement, etc.).

However, it should be remembered that this study is limited to simple structural elements. We propose simplified boundary conditions and they are therefore questionable: they do not take into account the behaviour of the soil or the foundation and are thus much more rigid than implementation of the structure requires. Therefore, a damaged structure is not necessarily destroyed, and can sometimes be repaired, which may involve a policy of planned maintenance.

Finally, this study is restricted to one part of the structure. We cannot yet deduce a damage indicator for the overall structure. This degree, between 0 and 1, from the absence of damage to the total loss of resistance, has become particularly common in earthquake engineering. However, given the different types of indicator identified, it does not seem relevant to the outcome of this study and requires continued research.

Nevertheless, despite the limits of this study, the conclusions indicate that it is advantageous to take the life of the structure into account. Indeed, the roughness of the roof of the gallery depends on whether or not there is roof snow, whether or not this snow is new, whether there is grass, the roof has been filled by landslides, etc.

Acknowledgements

The authors would like to express their thanks to the Rhone-Alps Region, its Environment Cluster group, all the members of the OPALÉ research program (ANR PGCU 2005), and the VOR federation for financially supporting this research. The authors wish to particularly thank IC Tonello, who provided data on the design of the gallery, used to build the numerical model, and Philippe Berthet-Rambaud for the interesting discussions. The authors also thank Linda Northup for checking the English.

References

- [1] Badré D. Le génie paravalanche en France. *Rev For Fr* 1974;26(1):22–30.
- [2] Rapin F. Récapitulatif des techniques françaises de protection collective paravalanche: Cemagref/division ETNA. *revue de l'ANENA "Neige et Avalanches"* N° 55 – juin 91, Last update: 2002.
- [3] Nicot F, Gay M, Tacnet JM. JM Interaction between a snow mantle and a flexible structure: a new method to design avalanche nets. *Cold Reg Sci Technol* 2002;34(2):67–84.
- [4] OFROU 2007. 12007 Directive: actions d'avalanches sur les galeries de protection, 2007 V2.00. <http://www.astra.admin.ch>.
- [5] Thibert E, Baroudi D, Limam A, Berthet-Rambaud P. Avalanche impact pressure on an instrumented structure. *Cold Reg Sci Technol* 2008;54(3):206–15.
- [6] Berthet-Rambaud P, Limam A, Roenelle P, Rapin F, Tacnet JM, Mazars J. Back-analysis of the collapse of Tacconnaz reinforced concrete deflective walls by February 11th 1999 avalanche. *Cold Reg Sci Technol* 2007;47:16–31.
- [7] Sovilla B, Schaer M, Kern M, Bartelt P. Impact pressures and flow regimes in dense snow avalanches observed at the Vallée de la Sionne test site. *J Geophys Res* 2008;113:F01010. <http://dx.doi.org/10.1029/2006JF000688>.
- [8] Sovilla B, Schaer M, Rammer L. Measurements and analysis of full-scale avalanche impact pressure at the Vallée de la Sionne test site. *Cold Reg Sci Technol* 2008;51:122–37.
- [9] Baroudi D, Thibert E. An instrumented structure to measure avalanche impact pressure: error analysis from Monte Carlo simulations. *Cold Reg Sci Technol, Int Snow Sci Workshop (ISSW 2008)* 2009;59(2–3):242–50.
- [10] Ma Y Analyse de l'effet d'une avalanche de neige sur un ouvrage de protection type Galerie Paravalanche: Expérimentation – Modélisation, PhD thesis, Université de Savoie, 2008.
- [11] Ma Y, Perrotin P, Mommessin M, Mazars J. Measurement of the characteristics of a rapid dry granular flow. *Powders & grains conference*, Golden, CO, USA, July 13–17, 2009.
- [12] Platzer K, Bartelt P, Jaedicke C. Basal shear and normal stresses of dry and wet snow avalanches after a slope deviation. *Cold Reg Sci Technol Jul* 2007;49(1):11. <http://dx.doi.org/10.1016/j.coldregions.2007.04.003>.
- [13] Thibert E, Baroudi D. Impact energy of an avalanche on a structure. *Ann Glaciol* 2010;51(54):45–54.
- [14] Rouquand A, Pontiroli C, Gerstle W, Bazant ZP, Wittmann FH. Some considerations on implicit damage models including crack closure effects and anisotropic behaviour. In: *Proc. FRAMCOS-2*. Freiburg, Germany: AEDIFICATIO Publisher; 1995.
- [15] Pontiroli C, Rouquand A, Mazars J. Prédiction du comportement du béton du chargement statique aux impacts à haute vitesse. *Vue d'ensemble du modèle PRM*. *Eur J Environ Civil Eng* 2010;14(6–7):703–27. <http://dx.doi.org/10.3166/ejece.14.703-727>.
- [16] Lodygowski T, Jankowiak T. Identification of parameters of concrete damage plasticity constitutive model. *Found Civil Environ Eng* 2005;6:53–69.
- [17] Norem H, Kvisterøy T, Evensen BD. Measurement of avalanche speeds and forces: instrumentatio and preliminary results of the Ryggfonn project. *Ann Glaciol* 1985;6:19–22.
- [18] Berthet-Rambaud P, Mazars J, Daudeville L. Impact on a RC rock-shed slab/FEM modelling EURO-C 2006 computational modelling of concrete structures, Mayrhofen, Tyrol, Austria, 2006. p. 689–698.
- [19] Deschamps JD, Church J, Showers D. 2006 CBC Provo canyon snow shed proceedings of the 2006 concrete bridge conference held May 7–10, 2006 in Reno, Nevada.
- [20] Berthet-Rambaud P, Limam A, Baroudi D, Thibert E, Taillandier JM. Characterization of avalanche loading on impacted structures: a new approach based on inverse analysis. *J Glaciol* 2008;54(185):324–32.
- [21] Daudon D, Baroth J, Szczurowska P, Ma Y, Perrotin P. Finite element models and sensitivity analysis of the vulnerability of an avalanche protection gallery. *International snow and sciences workshop (ISSW09)*, Davos, Switzerland. 2009.
- [22] Naaim M, Faug T, Naaim-Bouvet F, Eckert N. Return period calculation and passive structure design at Tacconnaz avalanche path (France). *Ann Glaciol* 2010;51(54):89–97.
- [23] Shreider YA. *The Monte-Carlo method*. Pergamon Press; 1971.
- [24] Au SK, Beck JL. A new adaptative importance sampling scheme for reliability calculations. *Struct Saf* 1999;21:135–58.

- [25] Matthies HG, Brenner CE, Bucher CG, Guedes Soares C. Uncertainties in probabilistic numerical analysis of structures and solids – stochastic finite elements. *Struct Saf* 1997;19(3):283–336.
- [26] Stephanou G. The stochastic finite element method: past, present and future. *Comput Methods Appl Mech Eng* 2009;198(9–12):1031–51.
- [27] Baroth J, Bressolette P, Chauvière C, Fogli M. An efficient SFE method using Lagrange Polynomials: application to nonlinear mechanical problems with uncertain parameters. *Comput Methods Appl Mech Eng* 2007;196:4419–29.
- [28] Millard A, Gosse G, Heinfung G, Defaux G, Mohamed A. Reliability analysis of a reinforced concrete cooling tower, ASS-IACM 2000. In: Fourth international colloquium of shells and spatial structures, Chania, Crete, Greece, 2000.
- [29] Filippou FC, Constantinides M. FEDEASLab getting started guide and simulation examples, 2004. <http://www.fedeaslab.berkeley.edu>.
- [30] ABAQUS. Finite element code for mechanical analyses, versions 6.6–6.8, 2008. <http://www.abaqus.com>.
- [31] Bertrand D, Naaim M, Brun M. Physical vulnerability of reinforced concrete buildings impacted by snow avalanches. *Nat Hazards Earth Syst Sci* 2010;10:1531–45.
- [32] Voellmy A. Über die Zerstörungskraft von Lawinen. *Schweiz Bauzeitung Jahrg* 1955;73(12) [English translation by R.E. Tate, On the destructive force of avalanche: U.S. Department of Agriculture, Forest Service, Alta Avalanche Study Center, Translation No. 2, 1964].
- [33] Cemagref. Conseil Général de l'Isère, departmental road n°117, Montaulever snow shed recommendation for the design 2000.
- [34] Mazars J, Kotronis P, Ragueneau F, Casaux G. Using multifiber beams to account for shear and torsion: applications to concrete structural elements. *Comput Methods Appl Mech Eng* 2006;195(52):7264–81.
- [35] La Borderie C, Mazars J, Pijaudier-Cabot G. Damage mechanics model for reinforced concrete structures under cyclic loading. *ACI* 1994;134:147–72.
- [36] Menegotto M, Pinto P. Method of analysis for cyclically loaded reinforced concrete plane frames including changes in geometry and non-elastic behavior of elements under combined normal force and bending. In: IABSE symposium: resistance and ultimate deformability of structures acted on by well defined repeated loads – Lisboa, 1973. 328 p.
- [37] Kotronis P, Mazars J. Simplified modeling strategies to simulate the dynamic behaviour of R/C walls. *J Earthquake Eng* 2005;9(2):286–306.
- [38] Margreth S, Platzer K. New findings on the design of snow sheds. In: International symposium on mitigative measures against snow avalanches, Egilsstaðir, Iceland, March 11–14, 2008.
- [39] Humbert J, Baroth J, Daudeville L. Probabilistic analysis of a pull-out test. *Mater Struct* 2010;43:345–55.
- [40] Nicot F, Limam A. Neige, paravalanche et constructions Hermes ISBN: 978-2-7462-2975-4 2011.